Oxygen doping tuning in superconducting oxides by thermal annealing and hard X-ray irradiation

Oxygen doping tuning in superconducting oxides by thermal annealing and hard X-ray irradiation

Lorenzo Mino[1,*], Elisa Borfecchia[2], Angelo Agostino[2,3], Carlo Lamberti[2,3,4] and Marco Truccato[1,3]

[1]Department of Physics, Interdepartmental Centre NIS, University of Torino, Torino, Italy.
[2]Department of Chemistry, Interdepartmental Centre NIS, University of Torino, Torino, Italy.
[3]CrisDi Interdepartmental Center for Crystallography, University of Torino, Torino, Italy.
[4]IRC "Smart Materials", Southern Federal University, Rostov-on-Don, Russia.

*Corresponding author. E-mail address: lorenzo.mino@unito.it

Abstract

$Bi_2Sr_2CaCu_2O_{8+\delta}$ (Bi-2212) superconducting whiskers, owing to their microscopic size, are good candidates for the fabrication of miniaturized devices for production/sensing of THz-radiation based on their Intrinsic Josephson Junctions (IJJ) properties. With this respect, several studies demonstrated the possibility of controlling whisker IJJ parameters by modifying the oxygen content. In this paper we show that both thermal annealing and hard X-ray irradiation are effective ways to tune the oxygen doping. In particular, we monitored the effect of an annealing process at 363 K and of irradiation by 17 keV micro- and nano-beams on the structural and superconducting properties of selected Bi-2212 whiskers. Moreover we modeled by a finite element simulation the temperature field induced by the X-ray beam to try to clarify the origin of the measured changes.

Keywords

High-temperature superconductor; Bi-2212; synchrotron radiation; X-ray micro-/nano-beam; finite element method (FEM)

1 Introduction

Since a few years ago whisker-like crystals of $Bi_2Sr_2CaCu_2O_{8+\delta}$ (Bi-2212) [1, 2] attracted significant attention because of their very good crystalline quality, peculiar dimensions with micrometric cross sections, leading to high aspect ratios, and outstanding superconducting properties [3, 4].

The presence of a layered structure along the crystal c-axis, consisting of alternating superconducting and insulating planes, induces the intrinsic Josephson effect in this compound [5] and several studies have been published describing the possibility of producing or sensing coherent THz radiation using these materials [6-8]. Furthermore, some authors have reported on the possibility of controlling whisker intrinsic Josephson junction (IJJ) parameters (e.g. the critical current density and the junction resistance) by modifying the oxygen content, which is well known to be strongly related to the carrier density [9, 10].

Previous investigations by our group showed that the Bi-2212 whiskers can undergo an aging process when exposed to air at 273 K or to a helium atmosphere at room temperature for long periods (100 days) [11, 12], or when annealed at moderate temperature for few hours [13]. These processes are associated with oxygen depletion mechanisms, which lead to a modification of the *c*-axis length, and can be exploited to modulate the IJJ characteristics. Therefore a combined *in situ* structural and electrical characterization can help to better understand the ageing processes which can be crucial for the technological applications of these materials.

Also particle and photon irradiation has proven to be able to modify the structural and functional properties of these materials. The effect of heavy ion irradiation on Bi-2212 has been extensively investigated, showing that the critical temperature (T_c) starts to decrease when the fluences are higher than ~ $1 – 2 \times 10^{11}$ ions cm^{-2} [14]. Also electron irradiation can induce polycrystallinity and amorphization in the whiskers at fluences of ~ 10^{22} e^{-} cm^{-2} [15], whereas protons and α particles can knock O atoms out of the material at fluences of ~ 10^{16} particles cm^{-2}, affecting both T_c and the normal state resistivity [16].

Concerning photons, Ishibashi *et al.* [17] reported that γ-rays of about 1.3 MeV are able to induce the desorption of extra oxygen atoms from the BiO layers of Bi-2212 and to reduce the size of the crystallites. Also other studies highlighted that γ-rays with similar energy can modify the oxygen concentration and the carrier distribution in different high temperature superconductor compounds [18, 19]. In general, less energetic photons were considered unable to produce significant effects, but in the last decade great

improvements have been performed in the focusing of X-ray beams at synchrotron sources [20, 21], opening new possibilities for the study and manipulation of oxide superconductors [22, 23]. Recently we showed that it is possible to locally tune the oxygen doping content by irradiating the material with an intense 17 keV X-ray nano-beam [24] and this process can be exploited to fabricate electrical devices, paving the way to a novel X-ray nano-patterning method that in principle can be extended to all oxide materials [25].

In this paper we present a comparative study of the effect of an annealing process at 363 K and of hard X-rays irradiation by X-ray micro- and nano-beams on selected Bi-2212 whiskers. Since such treatments are expected to induce variations in the oxygen content in the micro-crystals, we monitored the *c*-axis parameter evolution by X-ray diffraction and we investigated the changes in the electrical properties.

2 Experimental

Samples synthesis. The Bi-2212 whiskers were grown starting from high purity commercial powders of Bi_2O_3, $SrCO_3$, $CaCO_3$ and CuO (Aldrich 99.9999%) finely mixed in Bi:Sr:Ca:Cu stoichiometric ratios of 1.5:1:1:2. The mixture was melted at 1050 °C and glassy plates were produced by quenching the melt between copper plates at room temperature. The growth of the crystals took place on the plates during a five day annealing at about 850 °C in a controlled O_2 flow. Such conditions were selected in order to obtain whiskers with doping features corresponding to the nearly optimally doped or slightly overdoped state to minimize the possible presence of defects due to oxygen vacant sites [26]. The Bi-2212 sample measured in the X-ray microprobe configuration has a size of 700 x 5.17 x 0.70 μm^3, while the whisker analyzed using the X-ray nanoprobe has a size of 600 x 13.6 x 1.59 μm^3.

Electrical measurements. The sample preparation procedure consists of the selection under an optical microscope (100× magnification) of a smooth and linear crystal. Then a chip which allows both electrical and structural measurements on the same crystal was obtained by mounting the whisker onto a sapphire substrate where four point contacts were obtained by Ag physical vapour deposition [27]. Such contacts were subsequently covered with Au to avoid oxidation and subjected to thermal diffusion at 450°C for 5 minutes in pure oxygen atmosphere. The SEM micrograph in Fig. 1d shows a typical whisker (the *c*-axis is perpendicular to the sapphire substrate) with its four contacts perpendicular to the crystal. Each sample was

electrically characterized along its *ab* crystallographic plane by the standard four-probe method with a 1 μA current.

X-ray micro- and nano-beam set-ups. The former ESRF ID22 beamline was installed on a high-β straight section of the ring equipped with two different undulators. After the front-end, the beam passed through the optics hutch (see Fig. 1a), where a set of selectable high-power filters and slits with adjustable horizontal and vertical apertures optimized the intensity and the shape of the beam. A flat horizontally deflecting Si mirror also allowed thermal load reduction and higher harmonic rejection, then the beam entered in a Kohzu fixed-exit Si(111) double crystal monochromator.

The microprobe set-up (experimental hutch EH1, see Fig. 1b) was based on Kirkpatrick-Baez (KB) mirrors that allowed us to reach a spatial resolution of 1.7 μm (vertical) × 5.3 μm (horizontal) with a photon flux I_0 = 10^9 photon s^{-1} at 17 keV. After passing in the micro-beam experimental hutch EH1, the beam entered in the nano-imaging experimental hutch EH2 (see Fig. 1c). The nano-focusing optics, located at 64 m from the undulator source, consisted of two graded multilayer coated surfaces mounted in crossed Kirkpatrick-Baez configuration. This design provided a reflectivity of 73% at 17 keV and a beam size of 117 (vertical) x 116 (horizontal) nm^2, with a photon flux I_0 = 1.9 x 10^{11} photon s^{-1} during our experiment. In both EH1 and EH2 experimental hutches different detectors were present: a mini-ionization chamber to monitor the intensity of the incoming beam, a Silicon Drift Detector (SDD) to acquire the XRF signals and a FreLoN CCD detector to collect micro-/nano-XRD patterns in transmission mode [28].

The chip holding the Bi-2212 whisker was alternately mounted in the ID22 hutch and in an off-line cryostat to allow complementary micro-/nano-XRD and electrical characterization on the same micro-crystal.

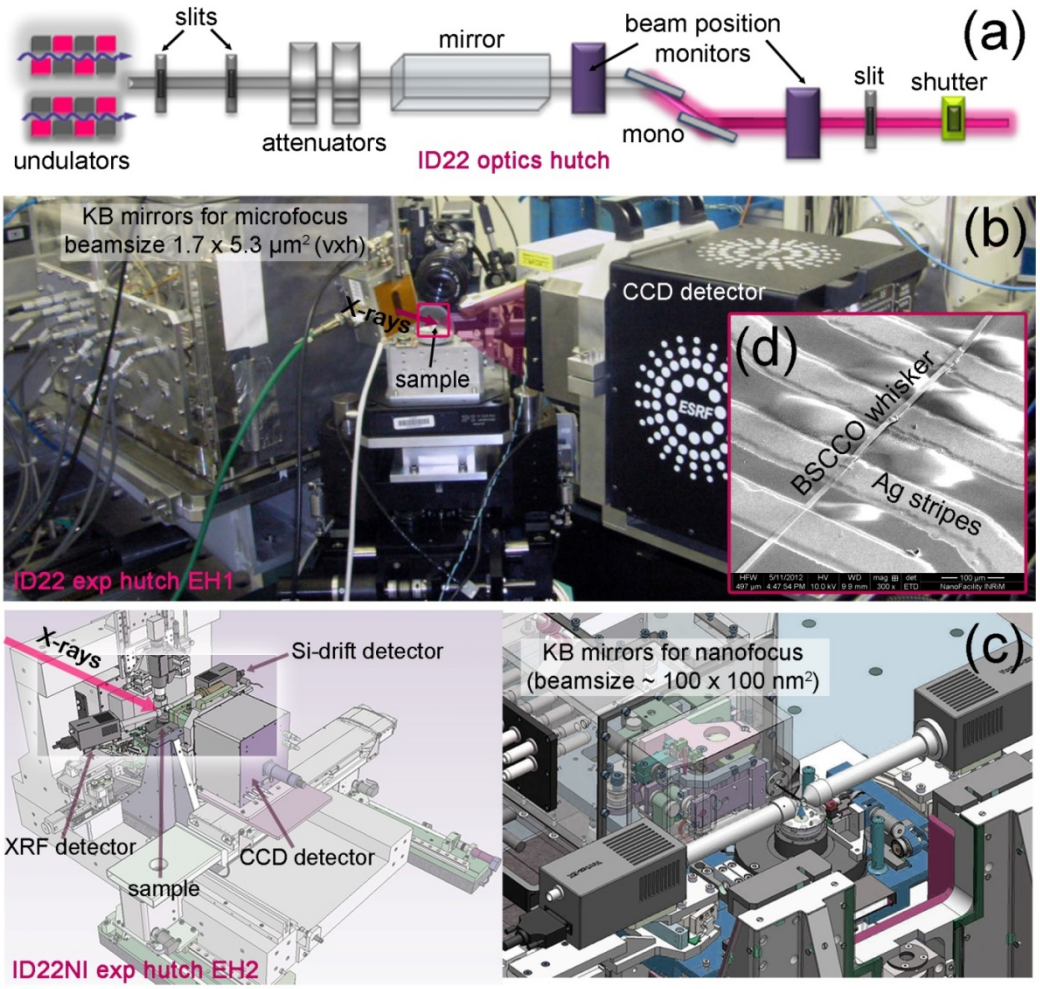

Fig. 1. (a) Scheme of the optics hutch of the former ESRF ID22 beamline, where the X-rays emitted by two undulators were monochromatized using two Si(111) reflections. (b) Photograph of the micro-beam experimental hutch EH1, containing the KB focusing mirrors, the rotating sample holder, the optical microscope for sample/beam alignment and the CCD camera to acquire the XRD patterns. (c) 3D scheme of the nano-beam experimental set-up used in the experimental hutch EH2 which is located after the hutch EH1. (d) Micrograph of a typical chip used for the measurements.

3 Results and discussion

3.1 Thermal annealing and micro-beam irradiation effects

The combination of resistivity versus temperature (R *vs* T) and micro-XRD measurements allowed firstly to clarify the effects of the exposure to hard-X ray micro-beam and the subsequent thermal annealing process on the oxygen content in an individual Bi-2212 whisker. Indeed, the evaluation of both electrical (e.g. the critical temperature T_c for the superconducting transition and the normal state resistivity ρ) [9, 10, 29] and structural parameters, primarily the *c*-axis length [10], allows to obtain detailed information on the oxygen

content, which is nearly proportional to the carrier density in the superconducting cuprate. In particular, for the *c*-axis and ρ values a monotonous increase is expected upon oxygen depletion. Conversely, the T_c value increases while moving from overdoped to optimally-doped Bi-2212, reaches its maximum in correspondence of the optimal doping condition (~ 2.2 x 10^{21} carriers/cm^3) and then decreases entering the underdoped regime [9, 10, 29]. With this respect, we employed the X-ray micro-probe of the former ESRF ID22 beamline to compare the impact of X-ray exposure to the effect of the thermal annealing on the local structural features of the Bi-2212 whiskers.

As discussed in a previous study [13] and hereinafter summarized, the significant *c*-axis elongation observed after a 6 h annealing at 363 K correlated with the modifications detected in the electrical properties, globally evidencing a decrease in the oxygen content from almost optimally doped to underdoped, for the as-grown and annealed whisker, respectively [13]. However, more detailed insights on the mechanism underlying the oxygen depletion process can be obtained considering also the oxygen doping modification induced by the micro-beam, whose properties are reported in Section 2.

It is worth noting that, in order to allow a quantitative comparison between the different X-ray irradiation conditions that we tested, including micro-beam and nano-beam (*vide infra*, Section 3.2) exposures, the dose D can be calculated according to eq. (1):

	$D = \frac{I_0\ \Delta t\ E_{abs}}{m_{I_0}} = \frac{I_0\ \Delta t E_0\,(1 - e^{-\frac{t}{\lambda_a}})}{V_{I_0}\rho_m}$	(1)

where Δ*t* is the total time of irradiation, E_{abs} the absorbed photon energy, m_{I0} the irradiated mass of Bi-2212, V_{I0} the irradiated volume, ρ_m the mass density, *x* the material thickness and λ_α the attenuation length of photons in Bi-2212, whose value is λ_α =17.38 μm at the energy E_0 = 17 keV [30].

In particular, the X-ray micro-beam irradiation was performed by multiple raster scans of the micro- probe on a region of 150 × 5.17 μm^2 of the whisker, resulting in a dose D = 7.5× 10^7 Gy, as reported in Fig. 2.

Let us first discuss the evolution of the electrical behaviour of the probed Bi-2212 whisker upon (i) X-ray micro-probe irradiation and (ii) subsequent thermal annealing. The results obtained from electrical characterization are summarized in Fig. 2, reporting R *vs* T curves measured on the as-grown sample, after exposure to the X-ray micro-beam, and finally after annealing the crystal at 363 K in air for 6 hours.

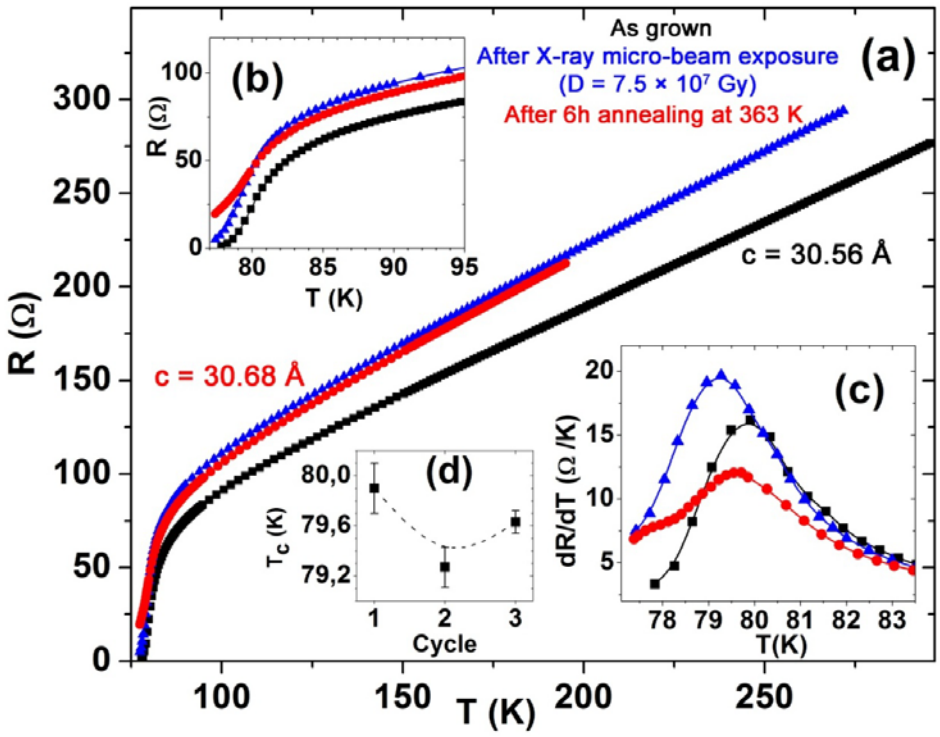

Fig. 2. (a) Four-probe R *vs* T curves for the as-grown sample (black squares), after exposure to the X-ray micro-beam (blue triangles), and after a subsequent annealing of 6 h at 363 K in air (red circles). (b): Magnified view of the transition region. (c): Derivatives of the curves of panel (a). (d): Critical temperatures as determined from the peak values of the derivatives shown in panel (c). The error bars simply indicate the uncertainty in determining the peak positions and are not related with the transition width. The dashed line represents a guide to the eye. Unpublished Figure; the data for as-grown and annealed sample were previously reported in ref. [13].

Very interestingly, comparing the R *vs* T curves collected for the as-grown and X-ray irradiated sample, we observe a decrease in the critical temperature T_c (determined from the position of the first derivative peak of the R(T) curve, see Fig. 2c) by about 0.6 K. Correspondingly, an increase in the normal state resistance by about 15% is observed. These evidences point out an X-ray induced reduction in the doping level of the crystal [10, 29], which moves from an almost optimally doped condition towards a slightly underdoped one. It should also be considered that, in agreement with previously reported results obtained for a different micro-crystal from the same synthesis batch [31], the electrical characterization clearly confirms that hard X-ray irradiation induces significant modifications in the superconducting and in the normal state behaviour of the investigated Bi-2212 whisker. All of these evidences can be consistently related to a local oxygen-depletion mechanism, involving a rearrangement of the O-atoms distribution in the irradiated area. Similar results were also reported for a Y-123 microbridge under irradiation by 20 keV electrons [32]. The observed

increase in the resistivity was explained by Tolpygo *et al.* by a knock-out of the loosely bound O-atoms by the incident electron beam. According to this interpretation, irradiation likely induces a disordering effect within the irradiated regions, resulting in a local lowering in the doping level without oxygen diffusion out of the material. A similar process based on the displacement of interstitial oxygen atoms in the Bi-2212 by the secondary electrons produced upon irradiation with high doses of 17-keV photons is very likely to play a role in our experiment.

The subsequent annealing of the crystal seems to partially restore the pristine conditions of the material. Indeed, the corresponding curve shown in Fig. 2 indicates a reduction of about 2% in the normal state resistance and an increase of about 0.4 K in T_c, with respect to the values observed after X-ray micro-beam exposure. This observation supports the hypothesis of a previous local-scale lowering of oxygen content because thermal annealing drives back the system towards an equilibrium state corresponding to a higher oxygen amount. However, as illustrated in Fig. 2b, the R(T) curve collected after annealing globally displays a significantly modified shape. In particular, the annealed whisker is characterized by a widened superconducting transition, as confirmed by the corresponding derivative plot reported in Fig. 2c. In these conditions the formation of a new minor phase, exhibiting a lower T_c, seems likely, as also suggested in previous XRD observations of thermally annealed Bi-2212 crystals [33].

As previously introduced, the *c*-axis length has been identified as a particularly sensitive indicator for the doping level [10], hence it has been monitored for the as-grown sample and for the final step of the treatment, *i.e.* after X-ray exposure and annealing. In particular, once the whisker was suitably aligned, single-crystal (00*l*) diffraction peaks were detected. The analysis of these XRD data resulted in a significant increase of the *c*-axis value determined for the sample after micro-beam irradiation and subsequent annealing, which lengthens to 30.68 Å from the 30.56 Å value for the almost optimally doped as-grown material. The final *c*-axis value of 30.68 Å, typical of underdoped Bi-2212 [10], definitely confirmed the overall oxygen-depletion effect cumulatively produced by combined X-ray irradiation and thermal treatment.

When considering these combined effects of X-rays and thermal annealing, it should be considered that many authors [10, 13, 31] have already shown that thermal treatment is an effective process to induce oxygen depletion and related tuning of the electrical properties in Bi-2212 whiskers. For this reason, before associating an independent mechanism to the modifications induced by X-ray irradiation, the possibility of

local temperature increase induced by the final phononic decay of the power deposited by the highly focused X-ray beams in the material has to be considered. Indeed, a significant increase in the local temperature upon irradiation could promote oxygen out-diffusion, equivalently to the annealing process but on a more local scale. To evaluate this scenario we have built a 3D finite element model (FEM), where the heating process induced by the X-ray beam on the sample is simulated for all the experimental conditions, thus corresponding to micro- and nano-beam irradiation (see Section 3.3).

3.2 Nano-beam irradiation effects

The use of a X-ray nano-beam, which ensures an even higher photon density (~ 10^7 ph s^{-1} nm^{-2}), enabled us to enhance the irradiation effect and therefore achieve deeper insights in the nature of the X-ray induced oxygen depletion mechanism. The nano-beam experiment was performed at the former ESRF ID22 beamline, like the previous study of the combined effect of micro-beam exposure and thermal annealing. However, here we employed the improved focusing capabilities of the nano-imaging experimental hutch (see Section 2 for details), simultaneously allowing a higher spatial resolution and a higher photon flux in pink beam mode. As for the micro-beam experiment discussed before, the X-ray energy was set to 17 keV. The selected sample was irradiated in air at room temperature, in three subsequent steps, corresponding to increasing X-ray doses, quantified in ~ 1.7×10^{11} Gy, 19×10^{11} Gy and 32×10^{11} Gy, according to eq. (1). An individual irradiation step consisted in a raster scan of the sample, covering all the width of the crystal for 30 μm in the [100] direction in a region located between the voltage contacts, with the beam parallel either to the [001] or to the [010] direction. In this experiment, we carefully monitored the variation of the *c*-axis and of the R *vs* T curves after each irradiation step, as summarized in Fig. 3.

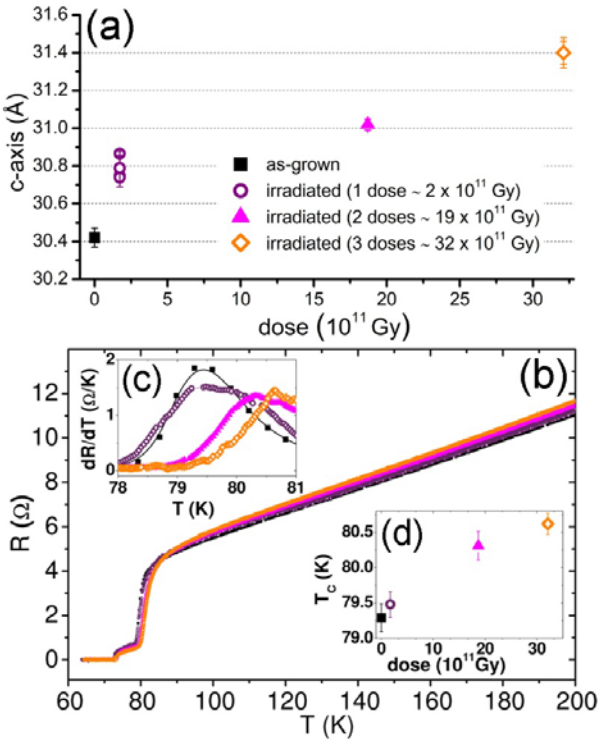

Fig. 3. Summary of the results obtained from combined structural and electrical characterization on an individual Bi-2212 whisker upon a three-step X-ray nano-beam irradiation process. (a) *c*-axis values obtained from nano-XRD characterization of the as-grown sample and after exposure to increasing X-ray doses. (b) Corresponding four-probe in-plane R *vs* T curves, showing the electrical response for the as-grown sample and after each one of the three irradiation steps. Error bars on R ($\sigma_R \approx \pm 0.02\ \Omega$) are negligible on the scale of this figure, hence are omitted. (c) Analysis on the first order derivative of R(T) to determine the mid-point transition temperature for the Bi-2212 main phase; its variation as a function of the dose is displayed in panel (d).

In particular, Fig. 3a reports the *c*-axis evolution as monitored by nano-XRD measurements. A monotonous increase of the lattice parameter is evident with increasing X-ray doses. This result provides a direct structural evidence of a local reduction in the carrier density upon 17 keV photons irradiation, complementing the preliminary insights obtained from the electrical characterization of the micro-beam exposed whisker discussed above. With respect to electrical measurements, Fig. 3b reports the R *vs* T curves acquired for the as-grown whisker and after the three subsequent X-ray doses. Firstly, it is worth noting that the four R(T) curves are characterized by the presence of two distinct transitions. The main one is associated to the Bi-2212 nominal phase, with a critical temperature T_c around 80 K, whereas the additional transition observed below 75 K can be related to the top layers of material chemically modified by the silver diffused from the uppermost electrical contacts [34]. The T_c of the principal transition, determined for the main Bi-

2212 phase from the position of the maximum in the first derivative curve plotted in Fig. 3c, are reported in Table S1, in correspondence of the increasing X-ray doses tested.

A first experimental consequence of material irradiation is the progressive increase of the mid-point transition temperature (Fig. 3d). In particular, the as-grown sample exhibits a T_c of (79.29 ± 0.20) K, which, combined with the *c*-axis value of (30.42 ± 0.05) Å, suggests an overdoping condition in the pristine material. A remarkable T_c increase is observed after the three X-ray doses, corresponding to a *c*-axis value of (31.40 ± 0.08) Å. Intermediated values are reached in correspondence of the first and second irradiation steps, evidencing a less-than-linear growth trend for the T_c as a function of the dose. Finally, the monotone increase of T_c suggests that the global X-ray irradiation process promoted the transition from an overdoped to an almost optimally-doped condition in the exposed whisker, without passing the maximum in the T_c *vs* carrier density curve.

In addition, a progressive increase in the normal state resistance is observed upon increasing X-ray doses, (Fig. 3, see in particular the high temperature behaviour of the four reported R(T) curves). The combination of the T_c and resistance evolution upon irradiation results in the intersection of all the four collected R(T) curves at about 85 K. The resistance increase is in agreement with the *c*-axis elongation found *via* nano-XRD in correspondence of increasing X-ray doses, definitely demonstrating that the X-ray irradiation induces an oxygen depletion phenomenon.

3.3 Finite element simulation of the micro-/nano-beam heating effect

Hereinafter we describe for both the micro- and the nano-beam set-ups a 3D model where the equation of heat is implemented to investigate if a significant increase in the local temperature is produced upon irradiation. The physical phenomena considered for the heat transfer process are conduction and convection, in a stationary state at the initial temperature of 300 K. Thus, the energy balance can be expressed by the following partial differential equation, eq. (2):

	$\nabla \cdot (-k\nabla T) + \rho_m C_p \vec{u} \cdot \nabla T = Q$	(2)

where *k* is the thermal conductivity, *T* is the temperature, ρ is the mass density, C_p is the heat capacity, $\vec{u}$ is the air velocity and *Q* represents the heat source. The latter is expressed as the average power per unit

volume dissipated inside the crystal and is determined considering the fraction of energy absorbed by the material, according to eq. (3):

	$$Q = \frac{P_{abs}}{V} = \frac{I_0 E_0 \eta}{V}$$	(3)

where P_{abs} is the absorbed power, η the fraction of absorbed intensity and V the volume of the source. The ratio of energy released within a distance x inside the material is finally given by eq. (4):

	$$\eta = \frac{E_{abs}}{E_0} = 1 - e^{-\frac{x}{\lambda}}$$	(4)

As a first approximation, V is the total volume defined by the intersection between the beam and the crystal, and the energy absorbed is assumed to be homogeneously distributed in such a volume.

Using the expressions written above it is possible to obtain all of the input data necessary to build the geometrical and physical model, as summarized in Table S2.

In both micro- and nano-beam configurations, the geometrical model was built employing the effective sample dimensions, reported in Section 2 for the two investigated whiskers. From top to bottom, the model includes: (i) the superconducting crystal; (ii) a 1 μm-thick layer of air; (iii) a 200 μm-thick sapphire substrate, which is in contact with the crystal through 2 sapphire pads of the same height of the air layer, located below the crystal extremities. An air volume (200 μm thick) surrounds the crystal, to include the effect of air convection in the thermal energy balance. Considering the large volume of the sapphire substrate with respect to the volume of the crystal, a constant temperature of 300 K was set as a boundary condition in the sapphire bottom and side faces. The physical parameters for the materials of interest employed to implement the FEM simulations are summarized in Table S3. The computer simulations were performed using the release 4.3a of the commercial software COMSOL Multiphysics®.

The resulting temperature field distributions induced by the synchrotron micro-beam and nano-beam are reported in the top and bottom panels of Fig. 4, respectively. In both cases only the experimental configuration with the X-ray beam parallel to the [001] direction has been reported for homogeneity.

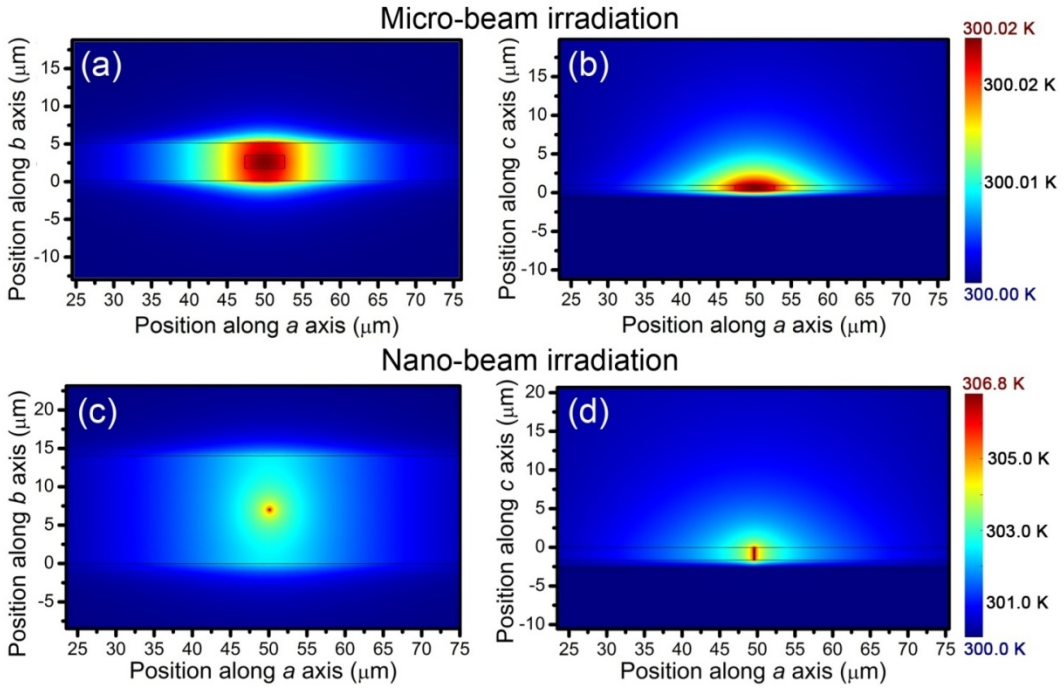

Fig. 4. Simulated temperature field distribution induced by the synchrotron micro-beam (top panels) and nano-beam (bottom panels). Panels (a) and (c) refer to the plane perpendicular to the [001] direction, crossing the whiskers in the middle of their thickness. Panels (b) and (d) refer to the plane perpendicular to the [010] direction, passing through the centre of the beam. In panels (a) and (b) the lines corresponding to the boundaries of the micro-crystals are also visible.

Panels (a) and (b) in Fig. 4 clearly show that the increase in temperature induced by the X-ray micro-beam is very feeble, both in transversal and longitudinal directions. In particular, the maximum temperature variation evaluated by FEM simulation is of only 0.02 K. The nano-beam configuration induces a slightly more effective heating effect, as illustrated in Fig. 4c,d. Indeed, in this case the maximum temperature increase is of 6.8 K, observed at the source position. The thermal perturbation extends from the source location up to about 20 μm along the *a*-axis of the crystal and exceeds the crystal edges along *b*- and *c*-axis: thereby, part of the power is dissipated through convection by the air surrounding the sample. A direct quantitative comparison between the two simulations is not straightforward, due to the different conditions considered. In particular, the two crystals differ in thickness and a different incoming photon flux is employed: both of these two factors significantly influence the amount of power density of the heat source, reflecting the different experimental conditions related to the micro- and nano-beam configurations. Nevertheless, the simulated phenomena are representative of the X-ray irradiation experiments discussed in the previous Sections, and point out a minor thermal effect of the X-ray irradiation, suggesting that other microscopic

mechanisms have to be considered for possible explanation of our experimental evidences, like for instance the oxygen knock-out by the secondary electrons locally produced by the X-rays. However, it should be underlined that these simulations are performed in stationary conditions, using a time-averaged power density. Since the synchrotron beam is pulsed, the instantaneous power density can be considerably higher, thus inducing higher local temperature increases for very short time scales.

4 Conclusions

In this paper we reported a comprehensive study of the effect of an annealing process at 363 K and of hard X-rays irradiation on selected Bi-2212 whiskers. By combining *in situ* synchrotron micro- and nano-XRD and electrical characterizations, we monitored the changes in structural and superconducting properties associated to such processes.

We showed that the structural effect of the micro-beam irradiation followed by a 6 h annealing at 363 K is to gradually increase the *c*-axis length. This result, correlated with the modifications detected in the electrical properties, globally evidences a decrease in the oxygen content in the Bi-2212 whisker which is initially almost optimally doped and progressively becomes underdoped.

In the case of nano-beam irradiation, we measured a progressive increase of the mid-point transition temperature from (79.29 ± 0.20) K to (80.62 ± 0.15) K after three steps of irradiation (total dose = 32 x 10^{11} Gy). Moreover, a gradual increase in normal state resistance is observed upon increasing X-ray doses. In parallel, we noticed a progressive *c*-axis elongation which confirms that the X-ray irradiation induces an oxygen depletion phenomenon.

To better understand the origin of the measured changes, we employed a 3D finite element model to calculate the temperature field distributions induced by the X-ray micro- and nano-beams. The maximum temperature variation evaluated by the FEM simulation is of 6.8 K for the nano-beam configuration and only of 0.02 K for the micro-beam set-up, suggesting the presence of other mechanisms responsible for oxygen decrease, e.g. oxygen knock-out by the secondary electrons locally produced upon X-ray irradiation. However, further simulations taking into account the temporal structure of the incoming synchrotron beam (i.e. the time-dependent power density) should be performed.

Acknowledgements

The authors gratefully acknowledge technical support from Nanofacility Piemonte at INRIM-National Institute for Metrological Research, with the financial contribution of Compagnia di San Paolo. Dr. G. Martinez-Criado is gratefully acknowledged for her competent and important support during the experiments at the former ID22 beamline of the ESRF. This work has been partly carried out under project NANO-X jointly approved and funded by University of Torino and Compagnia di San Paolo. C.L. thanks the Russian Ministry of Education and Science for the support (megagrant of the Russian Federation Government no. 14.Y26.31.0001).

References

[1] I. Matsubara, H. Tanigawa, T. Ogura, H. Yamashita, M. Kinoshita and T. Kawai, Jpn. J. Appl. Phys. 2, 28 (1989) L1358-L1360.

[2] I. Matsubara, H. Tanigawa, T. Ogura, H. Yamashita, M. Kinoshita and T. Kawai, Appl. Phys. Lett., 58 (1991) 409-411.

[3] Y.Q. Zhou, Z.J. Chen, H. Jin, P. Zheng and W.H. Wang, J. Cryst. Growth, 204 (1999) 289-292.

[4] P. Badica, K. Togano, S. Awaji, K. Watanabe and H. Kumakura, Supercond. Sci. Tech., 19 (2006) R81-R99.

[5] R. Kleiner, F. Steinmeyer, G. Kunkel and P. Muller, Phys. Rev. Lett., 68 (1992) 2394-2397.

[6] L. Ozyuzer, A.E. Koshelev, C. Kurter, N. Gopalsami, Q. Li, M. Tachiki, K. Kadowaki, T. Yamamoto, H. Minami, H. Yamaguchi, T. Tachiki, K.E. Gray, W.K. Kwok and U. Welp, Science, 318 (2007) 1291-1293.

[7] L. Ozyuzer, Y. Simsek, H. Koseoglu, F. Turkoglu, C. Kurter, U. Welp, A.E. Koshelev, K.E. Gray, W.K. Kwok, T. Yamamoto, K. Kadowaki, Y. Koval, H.B. Wang and P. Muller, Supercond. Sci. Tech., 22 (2009) 114009.

[8] T.M. Benseman, A.E. Koshelev, W.K. Kwok, U. Welp, V.K. Vlasko-Vlasov, K. Kadowaki, H. Minami and C. Watanabe, J. Appl. Phys., 113 (2013) 5.

[9] T. Kawae, K. Inomata, S.J. Kim, Y.I. Latyshev, K. Nakajima, T. Yamashita, S. Kishida and T. Hatano, Supercond. Sci. Tech., 14 (2001) 1102-1105.

[10] K. Inomata, T. Kawae, K. Nakajima, S.J. Kim and T. Yamashita, Appl. Phys. Lett., 82 (2003) 769-771.

[11] M. Truccato, S. Cagliero, A. Agostino, M. Panetta and G. Rinaudo, Supercond. Sci. Tech., 19 (2006) 1003-1009.

[12] S. Cagliero, A. Agostino, E. Bonometti and M. Truccato, Supercond. Sci. Tech., 20 (2007) 667-671.

[13] S. Cagliero, A. Piovano, C. Lamberti, M.M.R. Khan, A. Agostino, G. Agostini, D. Gianolio, L. Mino, J.A. Sans, C. Manfredotti and M. Truccato, J. Synchrotron Radiat., 16 (2009) 813-817.

[14] V. Hardy, J. Provost, D. Groult, M. Hervieu, B. Raveau, S. Durcok, E. Pollert, J.C. Frison, J.P. Chaminade and M. Pouchard, Physica C-Superconductivity and Its Applications, 191 (1992) 85-96.

[15] G. Aldica, F. Vasiliu, I.I. Geru and B.M. Puscasu, J. Supercond., 13 (2000) 623-631.

[16] S.K. Bandyopadhyay, P. Barat, P. Sen, A.K. Ghosh, A.N. Basu and B. Ghosh, Phys. Rev. B, 58 (1998) 15135-15145.

[17] T. Ishibashi, O. Yoda and S. Goda, Physica C-Superconductivity and Its Applications, 228 (1994) 379-382.

[18] H. Ozkan, N.M. Gasanly and T. Kayed, Supercond. Sci. Tech., 13 (2000) 161-164.

[19] A. Kumar, P. Kumar, M.R. Tripathy, A.K. Arora and R.P. Tandon, Mater. Chem. Phys., 97 (2006) 230-235.

[20] G. Martinez-Criado, E. Borfecchia, L. Mino and C. Lamberti, in C. Lamberti and G. Agostini (Editors), Characterization of Semiconductor Heterostructures and Nanostructures (Second Edition), Elsevier, Amsterdam, 2013, p. 361-412.

[21] Y. Suzuki and Y. Terada, in J.A. van Bokhoven and C. Lamberti (Editors), X-Ray Absorption and X-Ray Emission Spectroscopy: Theory and Applications, John Wiley & Sons, Chichester (UK), 2016, p. 251-279.

[22] N. Poccia, M. Fratini, A. Ricci, G. Campi, L. Barba, A. Vittorini-Orgeas, G. Bianconi, G. Aeppli and A. Bianconi, Nature Materials, 10 (2011) 733-736.

[23] N. Poccia, M. Chorro, A. Ricci, W. Xu, A. Marcelli, G. Campi and A. Bianconi, Appl. Phys. Lett., 104 (2014).

[24] A. Pagliero, L. Mino, E. Borfecchia, M. Truccato, A. Agostino, L. Pascale, E. Enrico, N. De Leo, C. Lamberti and G. Martinez-Criado, Nano Lett., 14 (2014) 1583-1589.

[25] M. Truccato, A. Agostino, E. Borfecchia, L. Mino, E. Cara, A. Pagliero, N. Adhlakha, L. Pascale, L. Operti, E. Enrico, N. De Leo, M. Fretto, G. Martinez-Criado and C. Lamberti, Nano Lett., 16 (2016) 1669-1674.

[26] M.M.R. Khan, S. Cagliero, A. Agostino, M. Beagum, C. Plapcianu and M. Truccato, Supercond. Sci. Tech., 22 (2009) 085011.

[27] M. Truccato, G. Rinaudo, C. Manfredotti, A. Agostino, P. Benzi, P. Volpe, C. Paolini and P. Olivero, Supercond. Sci. Tech., 15 (2002) 1304-1310.

[28] L. Mino, D. Gianolio, G. Agostini, A. Piovano, M. Truccato, A. Agostino, S. Cagliero, G. Martinez-Criado, S. Codato and C. Lamberti, Adv. Mater., 22 (2010) 2050-2054.
[29] T. Watanabe, T. Fujii and A. Matsuda, Phys. Rev. Lett., 79 (1997) 2113-2116.
[30] Note1, The attenuation length value for Bi-2212 has been obtained from the Center for X-Ray Optics at LBNL website: http://henke.lbl.gov/optical_constants/atten2.html 2013.
[31] G. Aldica, S. Cagliero, A. Agostino, C. Lamberti and M. Truccato, Supercond. Sci. Tech., 24 (2011) 035009
[32] S.K. Tolpygo, J.Y. Lin, M. Gurvitch, S.Y. Hou and J.M. Phillips, Phys. Rev. B, 53 (1996) 12462-12474.
[33] M. Truccato, A. Agostino, S. Cagliero, H. Motzkau, A. Rydh and V. Krasnov, World J. Eng., (2011) 1131-1132.
[34] Y.S. Luo, Y.N. Yang and J.H. Weaver, Phys. Rev. B, 46 (1992) 1114-1121.